

Distribution functions for the Milky Way

James Binney^{*}

Rudolf Peierls Centre for Theoretical Physics, Keble Road, Oxford OX1 3NP, UK

Draft, July 11, 2009

ABSTRACT

Analytic distribution functions (DFs) for the Galactic disc are discussed. The DFs depend on action variables and their predictions for observable quantities are explored under the assumption that the motion perpendicular to the Galactic plane is adiabatically invariant during motion within the plane. A promising family of DFs is defined that has several adjustable parameters. A standard DF is identified by adjusting these parameters to optimise fits to the stellar density in the column above the Sun, and to the velocity distribution of nearby stars and stars ~ 1 kpc above the Sun. The optimum parameters imply a radial structure for the disc which is consistent with photometric studies of the Milky Way and similar galaxies, and that 20 per cent of the disc's luminosity comes from thick disc. The fits suggest that the value of the V component of the Sun's peculiar velocity should be revised upwards from 5.2 km s^{-1} to $\sim 11 \text{ km s}^{-1}$. It is argued that the standard DF provides a significantly more reliable way to divide solar-neighbourhood stars into members of the thin and thick discs than is currently used. The standard DF provides predictions for surveys of stars observed at any distance from the Sun. It is anticipated that DFs of the type discussed here will provide useful starting points for much more sophisticated chemo-dynamical models of the Milky Way.

Key words: galaxies: kinematics and dynamics - The Galaxy: disc - solar neighbourhood

1 INTRODUCTION

A major thread of current research is work directed at understanding the origin of galaxies. There are excellent prospects of achieving this goal by combining endeavours in three distinct areas: observations of galaxy formation taking place at high redshift, numerical simulations of the gravitational aggregation of dark matter and baryons, and studies of the Milky Way. The latter field is dominated by a series of major observational programs that started fifteen years ago with ESA's Hipparcos mission, which returned parallaxes and proper motions for $\sim 10^5$ stars (Perryman 1997). Hipparcos established a more secure astrometric reference frame, and the UCAC2 catalogue (Zacharias et al. 2004) uses this frame to give proper motions for several million stars. These enhancements of our astrometric database have been matched by the release of major photometric catalogues [DENIS (Epchtein et al. 2005), 2MASS (Skrutskie et al. 2006), SDSS (Abazajian 2009)] and the accumulation of enormous numbers of stellar spectra, starting with the Geneva-Copenhagen Survey (Nordström et al. 2004; Holmberg et al. 2007, hereafter GCS) and continuing with the

SDSS, SEGUE (Yanny et al. 2009b) and RAVE (Steinmetz et al. 2006) surveys – on completion the SEGUE and RAVE surveys will provide 0.25×10^6 and $\sim 10^6$ low-dispersion spectra, respectively. These spectra yield good radial velocities and estimates of $[\text{Fe}/\text{H}]$ and $[\alpha/\text{Fe}]$ with errors of ~ 0.1 dex. Two surveys (HERMES and APOGEE) are currently being prepared that will obtain large numbers of medium-dispersion spectra from which abundances of significant numbers of elements can be determined. The era of great Galactic surveys will culminate in ESA's Gaia mission, which is scheduled for launch in late 2011 and aims to return photometric and astrometric data for 10^9 stars and low-dispersion spectra for $> 10^7$ stars.

The Galaxy is an inherently complex object, and the task of interpreting observations is made yet more difficult by our location within it. Consequently, the ambitious goals that the community has set itself, of mapping the Galaxy's dark-matter content and unravelling how it was assembled, can probably only be attained by mapping observational data onto sophisticated models. We are developing a modelling strategy that has as its point of departure analytic approximations to the distribution functions (DFs) of various components of the Galaxy (McMillan et al. in preparation). In this paper we present such approximations for the thin

^{*} E-mail: binney@thphys.ox.ac.uk

and thick discs. The paper is organised as follows. Section 2 explains how the DF is assembled. Section 3 compares the DF's predictions for various observables to data. In particular evidence is presented that the Sun's V velocity is conventionally underestimated by $\sim 6 \text{ km s}^{-1}$ and predictions are given for velocity distributions as a function of distance from the plane. Evidence is presented that the standard DF provides a cleaner division of solar-neighbourhood stars into members of the thin and thick discs than has been available hitherto. Section 4 sums up and looks ahead.

2 CHOICE OF THE DF

Our approach to Galaxy modelling starts from DFs that are analytic functions of the action integrals (J_r, J_θ, J_ϕ) of orbits in an integrable, axisymmetric Hamiltonian (McMillan et al., in preparation). The action J_ϕ associated with the azimuthal invariance of the Hamiltonian is simply the z component of angular momentum L_z , and the action denoted J_θ in Binney & Tremaine (2008; hereafter BT08), which quantifies motion perpendicular to the symmetry plane $z = 0$, is here conveniently denoted J_z . We shall be largely concerned with orbits that have sufficiently large values of L_z that a reasonable approximation to their dynamics can be obtained by considering the motion parallel to the plane to proceed regardless of the vertical motion, and the vertical motion to be affected by the motion in the plane only in as much as the latter causes the force perpendicular to the plane to vary in time slowly enough for the vertical motion to be adiabatically invariant – see BT08 §3.6.2(b) for a justification of this approximation. At any radius R we define the vertical potential

$$\Phi_z(z) \equiv \Phi(R, z) - \Phi(R, 0), \quad (1)$$

where $\Phi(R, z)$ is the full potential. Motion in Φ_z has the energy invariant

$$E_z(z, v_z) \equiv \frac{1}{2}v_z^2 + \Phi_z(z). \quad (2)$$

Given a value for E_z , the vertical action can be obtained from a one-dimensional integral

$$J_z(E_z) = \frac{2}{\pi} \int_0^{z_{\max}} dz v_z, \quad (3)$$

where $\Phi_z(z_{\max}) = E_z$.

Motion parallel to the Galactic plane is assumed to be governed by the radial potential

$$\Phi_R(R) \equiv \Phi(R, 0), \quad (4)$$

so the radial action is

$$J_r(E_R, L_z) = \frac{1}{\pi} \int_{R_p}^{R_a} dr v_R, \quad (5)$$

where R_p and R_a are the peri- and apo-centric radii and $v_R \equiv \sqrt{2(E_R - \Phi_R) - L_z^2/R^2}$.

Given a point in phase space, we can evaluate $L_z = J_\phi$, E_z and E_R and thus obtain J_r and J_z , so a given DF can be evaluated at any point in phase space.

We start from the simplest plausible DFs, which have the form

$$f(J_r, J_z, L_z) = f_1(L_z) f_r(J_r, L_z) f_z(J_z, L_z). \quad (6)$$

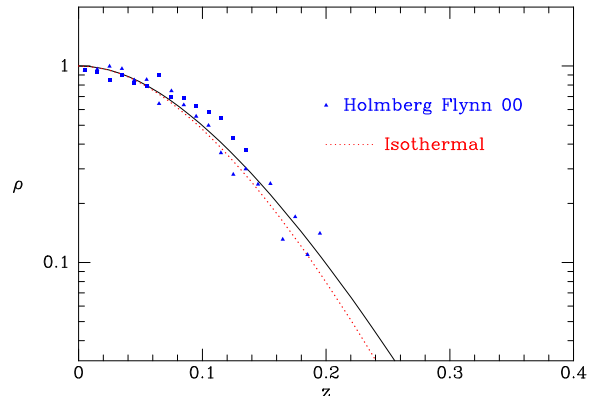


Figure 1. Comparison of the predictions of two theoretical models and the density of A (triangles) and F (squares) stars versus distance from the plane from Holmberg & Flynn (2000). The full curve is obtained from the DF (7) with $\sigma_z = 6.3 \text{ km s}^{-1}$ while the dotted curve is the classical exponential $\rho \propto \exp(-\Phi/\sigma_z^2)$ for the same velocity dispersion. The gravitational potential is that of Model II of §2.7 in BT08.

Here f_1 is primarily responsible for determining the surface density of the disc, f_r controls the degree of epicyclic motion within the disc, and f_z controls the disc's vertical structure. Since there is a close relation between a star's angular momentum L_z and the radii to which it contributes to observables, the appearance of L_z in f_r and f_z makes it possible for the disc to become hotter and/or thinner at small radii.

2.1 Vertical profiles

We now consider the form of the function f_z in equation (6), which controls the disc's vertical structure. We focus on motion in the solar cylinder of stars for which $L_z \simeq R_0 v_c(R_0)$ so they do not make large radial excursions. For these stars f_z is effectively a function of only J_z . The classical choice of DF is that of an isothermal sheet $f_z \sim e^{-E_z/\sigma_z^2}$ (Spitzer 1942). Our modelling strategy requires that we eliminate E_z in favour of J_z . In a separable potential $\Omega_z J_z = \langle v_z^2 \rangle$, where $\Omega_z = \partial E_z / \partial J_z$ is the vertical frequency and the angle brackets denote a time average along the orbit with action J_z . Moreover, by the virial theorem $\langle v_z^2 \rangle = E_z$ in a harmonic oscillator, so we replace E_z with $\Omega_z J_z$ and arrive at what we shall refer to as the “pseudo-isothermal” DF

$$f_{\sigma_z}(J_z) \equiv \frac{e^{-\Omega_z J_z / \sigma_z^2}}{2\pi \int_0^\infty dJ_z e^{-\Omega_z J_z / \sigma_z^2}}, \quad (7)$$

where the denominator ensures that f_{σ_z} satisfies the normalisation condition

$$\int dz dv_z f_{\sigma_z} = 1 \quad \Leftrightarrow \quad \int dJ_z f_{\sigma_z} = \frac{1}{2\pi}. \quad (8)$$

In general σ_z is a function of L_z to control the scale height as a function of radius, but for the moment we neglect this dependence and investigate the vertical density profile predicted by the DF (7) by taking $\Phi_z(z)$ to be the potential above the Sun in Model II of §2.7 in BT08; this model is disc dominated.

The full curve in Fig. 1 shows the density profile predicted by the DF (7) for $\sigma_z = 6.3 \text{ km s}^{-1}$, while the dotted

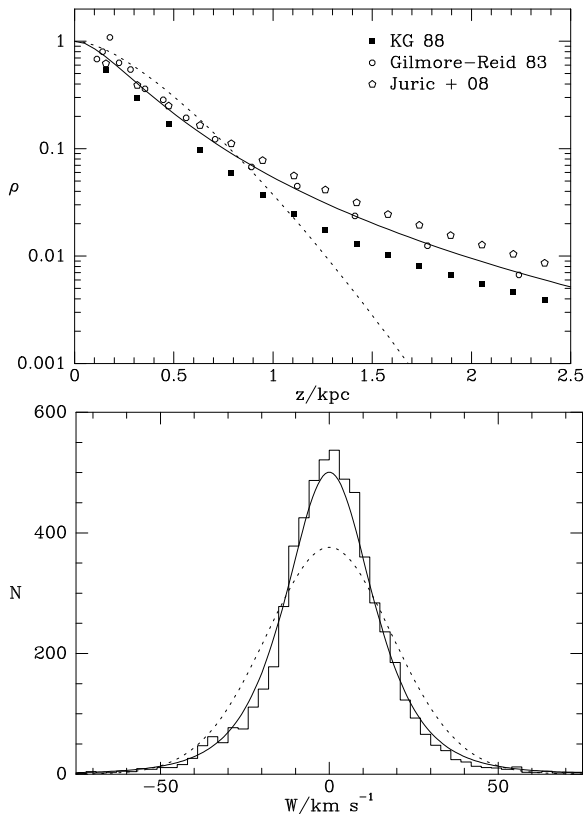


Figure 2. Upper panel: the full curve shows the vertical density profile predicted in the potential above the Sun by the DF of equation (9) with $\gamma = 2.6$ and $V_\gamma = 18.7 \text{ km s}^{-1}$. The dotted curve is the profile predicted by equation (7) with $\sigma_z = 18 \text{ km s}^{-1}$. The points show the density of main-sequence stars measured by Gilmore & Reid (1983), Kuijken & Gilmore (1989) and Juric et al. (2008). Lower panel: the full and dashed curves show the distributions in v_z at $z = 0$ predicted by the DFs of equations (9) and (7), while the histogram shows the distribution in v_z of the GCS stars.

curve shows the classical isothermal $\rho \propto \exp(-\Phi/\sigma_z^2)$. The two curves are very similar because equation (7) predicts that $\langle v_z^2 \rangle^{1/2}$ moves in a narrow range from 6.55 km s^{-1} at $z = 0$ to a peak value 6.7 km s^{-1} at $z = 240 \text{ pc}$. Both predictions are in reasonable agreement with the densities of A and F stars measured by Holmberg & Flynn (2000) shown by triangles and squares, respectively.

The dotted curve in the upper panel of Fig. 2 shows the vertical density profile predicted by equation (7) when $\sigma_z = 18 \text{ km s}^{-1}$. The curvature of the profile has the wrong sign to fit the density profile of dwarfs with $4 < M_V < 5$ measured by Gilmore & Reid (1983), which is shown by circles. The velocity dispersion in this model is $\langle v_z^2 \rangle^{1/2} = 19.2 \pm 0.3 \text{ km s}^{-1}$ independent of z , so the DF is very close to an isothermal. The dotted curve in the lower panel shows that the Gaussian distribution in v_z at $z = 0$ predicted by the DF is a poor fit to the distribution in v_z of the GCS stars.

One way to obtain a vertical profile that is steeper at small heights and flatter at large heights is to replace the exponential in equation (7) with an algebraic function of

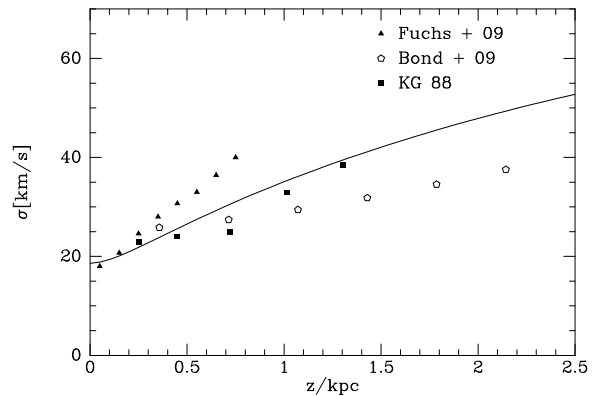


Figure 3. Velocity dispersion as a function of distance from the plane as predicted by the DF (9).

J_z . The full curves in Fig. 2 show the density profile and velocity distribution predicted by the DF

$$f_z(J_z) = \frac{(\Omega_z J_z + V_\gamma^2)^{-\gamma}}{2\pi \int_0^\infty dJ_z (\Omega_z J_z + V_\gamma^2)^{-\gamma}} \quad (9)$$

with $\gamma = 2.6$ and $V_\gamma = 18.7 \text{ km s}^{-1}$. The agreement with the data of Gilmore & Reid (1983) is essentially perfect. This fit, and all subsequent fits, were obtained by adjusting the parameters by hand and judging the quality of the fit by eye.

The curve in Fig. 3 shows the extent of the increase in velocity dispersion with height that is required to produce a thick-disc like flattening in the density profile at $z > 500 \text{ pc}$: $\langle v_z^2 \rangle^{1/2}$ rises from 19.6 km s^{-1} at $z = 0$ to 37.5 km s^{-1} at $z = 1 \text{ kpc}$ and 50.4 km s^{-1} at $z = 2 \text{ kpc}$. Also shown are three sets of data points: filled squares show the values of σ_z inferred by Kuijken & Gilmore (1989) (hereafter KG89) for the velocity dispersion of K dwarfs; filled triangles show the dispersion of metal-poor M dwarfs inferred by Fuchs et al. (2009); open pentagons show the analytic fit to the dispersions of disc stars that was published by Bond et al. (2009). Sadly, the data do not tell a coherent story. Each data set is for a different stellar population, so in principle their different trends in $\sigma_z(z)$ could be matched by different density profiles. Therefore in Fig. 2 we plot the density profiles associated with the Bond et al. sample (from Juric et al. 2008) and the KG89 sample. We see that the Juric et al. density profile is less steep than the one from KG89, which is inconsistent with the higher velocity dispersions measured by KG89. Fuchs et al. (2009) do not give a density profile, but it would be surprising if the kinematics and vertical structure of the M dwarfs were fundamentally different from that of the K dwarfs studied by KG89, so the extremely rapid increase in their values of $\sigma_z(z)$ shown in Fig. 3 is hard to understand.

The fact that the model curve in Fig. 3 agrees best with the KG89 may reflect the fact that the potential in which the DF is evaluated was constrained to be compatible with value for the surface density of material that lies within 1.1 kpc of the plane given by Kuijken & Gilmore (1991), which was based on the KG89 data. In a gravitational potential tailored for the data of Juric et al. (2008) and Bond et al. (2009) the DF might reproduce the data in these papers better than that of KG89. We do not pursue this question here.

Despite the simplicity of the DF (9) and the accuracy with which it fits the data, we will not employ it further because it does not provide a decomposition of the disc into populations of different ages, and there is no natural way of incorporating it into a DF that also describes the radial structure of the disc.

Star formation is known to have continued in the disc throughout the life of the Galaxy and the velocity dispersion of any cohort of coeval stars is known to increase secularly as a result of scattering by spiral arms and molecular clouds (Spitzer & Schwarzschild 1953; Carlberg & Sellwood 1985). Moreover, as the Galaxy ages, the chemical composition of the stars that are forming at a given radius changes, so stars formed at different times and different radii are in principle distinguishable. Hence it is useful to consider the disc's aggregate DF to be a sum of the DFs for stars of different ages and velocity dispersions.

We assume that the DF of stars of age τ is the ‘‘pseudo-isothermal’’ DF (7) with σ_z increasing with τ according to (e.g. Aumer & Binney 2009)

$$\sigma_z(\tau) = \sigma_{z0} \left(\frac{\tau + \tau_1}{\tau_m + \tau_1} \right)^\beta. \quad (10)$$

Here σ_{z0} is the velocity dispersion of stars at age $\tau_m \simeq 10$ Gyr, τ_1 sets velocity dispersion at birth, and $\beta \simeq 0.38$ is an index that determines how σ_z grows with age. If we further assume that the rate of star formation has declined with time as e^{-t/t_0} , then the aggregate DF will be

$$f_{\text{thn}}(J_z) = \frac{\int_0^{\tau_m} d\tau e^{\tau/t_0} f_{\sigma_z}(J_z)}{t_0(e^{\tau_m/t_0} - 1)}, \quad (11)$$

where σ_z depends on τ through equation (10). In Fig. 4 we plot the vertical density profile produced by this aggregate DF when $t_0 = 8$ Gyr, $\tau_1 = 0.1$ Gyr, $\sigma_{z0} = 20 \text{ km s}^{-1}$ (Aumer & Binney 2009). We see that with these parameters we obtain a reasonable fit to the thin disc. Specifically, at $z \gtrsim 150$ pc the density is nearly exponential with a scale height of 255 pc. In view of the dramatic difference between this pure thin-disc structure and the thin plus thick disc structure furnished by the algebraic DF (9), it is perhaps surprising that the velocity distribution in the lower panel of Fig. 4 differs as little as it does from the dashed curve in the lower panel of Fig. 2. This comparison illustrates an important point: thick-disc stars spend relatively little time near $z = 0$ so they contribute only inconspicuous wings to the velocity distribution there. The velocity distribution predicted by f_{thn} is close to Gaussian: the velocity dispersion rises from 16.5 km s^{-1} at $z = 0$ to 19.6 km s^{-1} at $z = 500$ pc and 20.9 km s^{-1} at $z = 1$ kpc.

Fig. 5 shows that a perfect fit to the Gilmore & Reid (1983) measurements can be obtained by adding a pseudo-isothermal component with $\sigma_z = 38 \text{ km s}^{-1}$ to the thin disc shown in Fig. 4. Within this structure $\langle v_z^2 \rangle^{1/2}$ increases from 19 km s^{-1} at $z = 0$ to 39 km s^{-1} at $z = 1.5$ kpc and then very slowly increases to 41.5 km s^{-1} at $z = 2.5$ kpc. It is worth noting that adding the thick disc increases the scale height in the exponential fit to the profile at low z from 255 pc to 336 pc.

2.2 Profiles within the plane

Shu (1969) discussed DFs for planar discs of the form

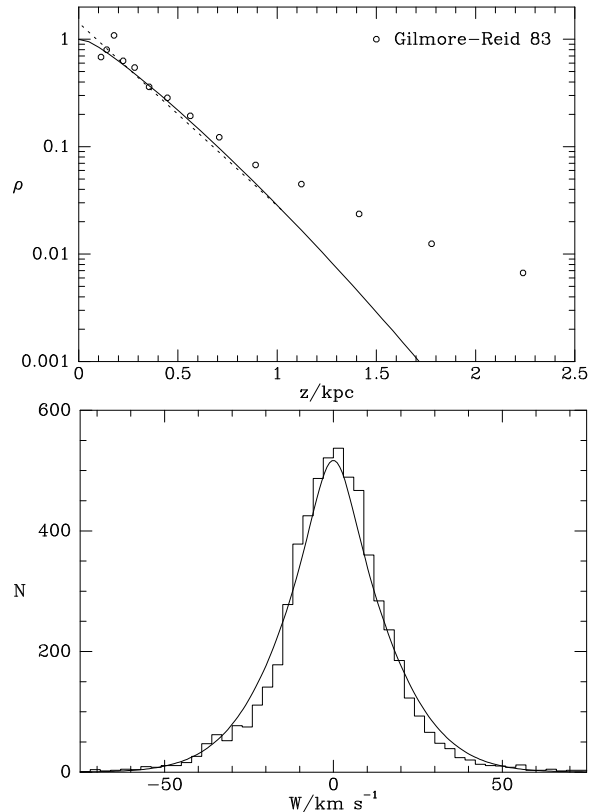


Figure 4. Full curves: the vertical density profile (upper panel) and the distribution of v_z (lower panel) predicted by the composite DF (11). Dashed line: an exponential of scale height 255 pc.

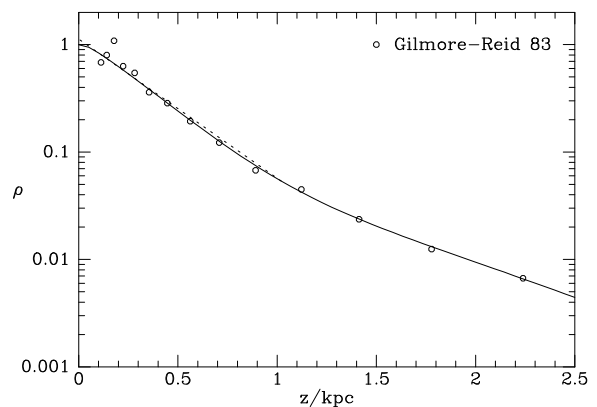


Figure 5. The result of adding to the composite thin disc of Fig. 4 a pseudo-isothermal disc with $\sigma_z = 38 \text{ km s}^{-1}$ that contains 20 percent of the total mass. The dashed line is an exponential with scale height 336 pc.

$$f_r(E, L_z) = e^{-(E-E_c)/\sigma_r^2}, \quad (12)$$

where $E_c(L_z)$ is the energy of a circular orbit of angular momentum L_z and $\sigma_r(L_z)$ is a function that determines the velocity dispersion in the disc as a function of radius. By analogy with the vertical DF we could replace $E - E_c$ by $\Omega_r J_r$, where $\Omega_r = \partial E / \partial J_r$ (Binney 1987; Dehnen 1999). However, the decrease in Ω_r as $J_r \rightarrow \infty$ is so rapid that for sufficiently eccentric orbits the product $\Omega_r J_r$ decreases with increasing J_r . Consequently, if one substitutes $\Omega_r J_r$ for

$E - E_c$, at fixed L_z and large J_r the DF increases with J_r . To prevent this unphysical behaviour we replace $E - E_c$ by κJ_r , where

$$\kappa(L_z) \equiv \lim_{J_r \rightarrow 0} \Omega_r(J_r, L_z) \quad (13)$$

is the epicycle frequency. Hence in this paper we adopt as the planar DF of a pseudo-isothermal population

$$f_r(J_r, L_z) = e^{-\kappa J_r / \sigma_r^2}. \quad (14)$$

In view of the normalisation condition (8), the mass dM placed by the DF (6) on orbits with angular momentum in the range $(L_z, L_z + dL_z)$ is

$$dM = (2\pi)^2 f_1 dL_z \int_0^\infty dJ_r e^{-\kappa J_r / \sigma_r^2} = (2\pi)^2 \frac{\sigma_r^2}{\kappa} f_1 dL_z \quad (15)$$

In the limit $\sigma_r \rightarrow 0$ of a cold disc, only circular orbits are populated and this mass is equal to the mass $2\pi R \Sigma dR$ in the annulus $(R, R + dR)$, where Σ is the disc's surface density. Hence for a cold disc

$$f_1(L_z) = \frac{\kappa R \Sigma}{2\pi \sigma_r^2} \frac{dR}{dL_z} = \frac{\Omega \Sigma}{\pi \sigma_r^2 \kappa} \bigg|_{R_c}, \quad (16)$$

where $R_c(L_z)$ is the radius of the circular orbit of angular momentum L_z and the second equality uses the identity $dL_z/dR = R\kappa^2/2\Omega$. Here we consider the case of an exponential disc, $\Sigma = \Sigma_0 e^{-(R-R_0)/R_d}$, where $R_d \simeq 2.5$ kpc is the scale length of the disc and $R_0 \simeq 8$ kpc is the Sun's distance from the Galactic centre. We assume that σ_r declines exponentially in radius with a scale length that is roughly twice that of the surface density

$$\sigma_r(L_z) = \sigma_{r0} e^{q(R_0 - R_c)/R_d} \quad \text{where } q \simeq 0.5. \quad (17)$$

This choice is motivated by naive epicycle theory, which implies that with $q \simeq 0.5$ the scale height will be constant (van der Kruit & Searle 1982) provided $\sigma_z/\sigma_r = \text{constant}$.

A DF such as f_1 times equation (14) that is an even function of L_z does not endow the Galaxy with rotation. We introduce rotation by adding to the DF an odd function of L_z , which will not contribute to either the surface density or the radial velocity dispersion. A convenient choice for this odd contribution to the DF is $\tanh(L_z/L_0)$ times the even contribution, where L_0 is a constant that determines the steepness of the rotation curve in the central region of solid-body rotation. At radii so large that $Rv_c \gg L_0$ this choice for the odd part of the DF simply eliminates counter-rotating stars. We choose $L_0 = 10 \text{ km s}^{-1} \text{ kpc}$, a value sufficiently small for counter-rotating stars to be confined to the inner kiloparsec of the Galaxy, which is in reality bulge-dominated. Hence we consider the ‘‘pseudo-isothermal’’ planar DF

$$f_{\sigma_r}(J_r, L_z) \equiv \frac{\Omega \Sigma}{\pi \sigma_r^2 \kappa} \bigg|_{R_c} [1 + \tanh(L_z/L_0)] e^{-\kappa J_r / \sigma_r^2}. \quad (18)$$

It is interesting to evaluate the observables predicted by the DF (18) when the circular speed is a power law in R , $v_c = v_0 (R/R_0)^\alpha$. Then

$$\Phi_R(R) = \frac{v_0^2}{\alpha} (R/R_0)^\alpha. \quad (19)$$

In the limit $\alpha \rightarrow 0$ of a perfectly flat circular speed

$$\Phi_R(R) = v_0 \ln(R/R_0). \quad (20)$$

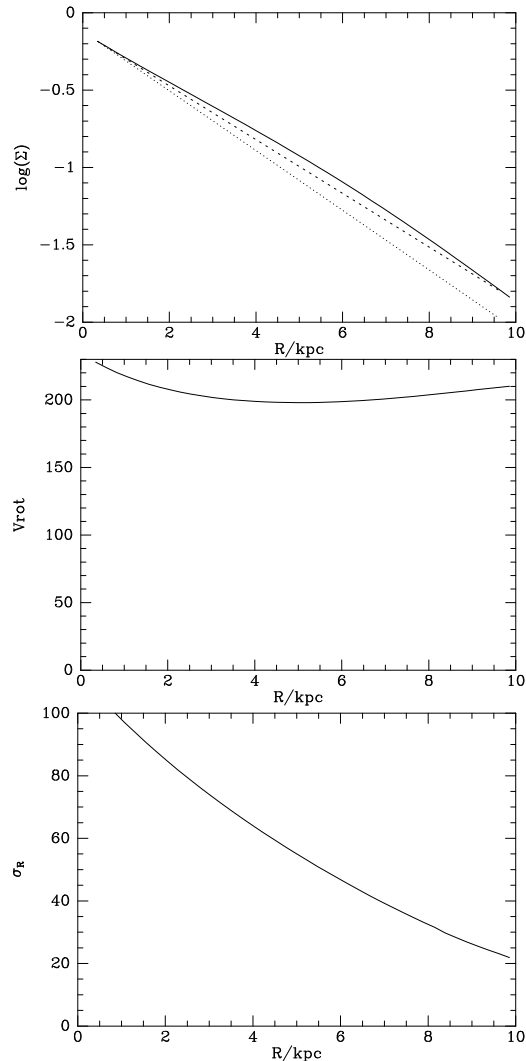


Figure 6. From top to bottom, the surface density, rotation speed and radial velocity dispersion obtained from the DF (18) when the gravitational potential is given by equation (20) with $v_0 = 220 \text{ km s}^{-1}$ and the velocity dispersion function is given by (17) with $\sigma_{r0} = 28.6 \text{ km s}^{-1}$ and $q = 0.45$. In the top panel the dashed line shows an exponential with scale length 2.5 kpc; in equation (18) $R_d = 2.25$ kpc was used but the recovered surface density profile is clearly shallower than the exponential with this scale length, which is shown by the dotted line.

Fig. 6 shows the surface density, rotation curve and radial velocity-dispersion profile predicted by the pseudo-isothermal DF (18) for a flat circular-speed curve with $v_0 = 220 \text{ km s}^{-1}$. For the plotted profiles the function $\Sigma(R_c)$ has been taken to be an exponential of scale length 2.25 kpc, while the full curve in the top panel shows that the surface density produced by this choice of $\Sigma(R_c)$ provides a good approximation to the surface density of an exponential disc with a longer scale length, 2.5 kpc, which is shown by the dashed line. At the price of replacing the analytic function

$$\Sigma(R_c) = e^{(R_0 - R_c)/R_d} \quad (21)$$

with a tabulated function, the surface density can be made exactly exponential (Dehnen 1999). Here we adopt the sim-

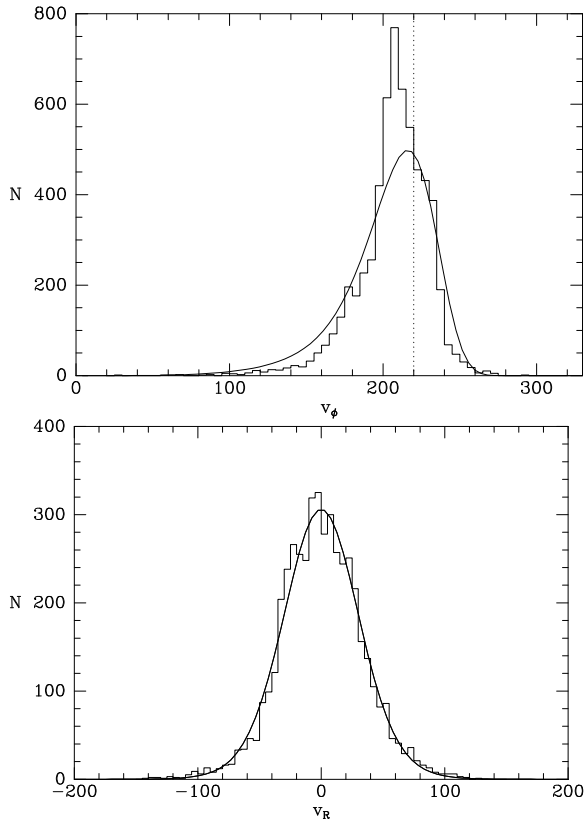


Figure 7. Comparison of the observed density of GCS stars in the (v_R, v_ϕ) plane with the prediction of the planar pseudo-isothermal DF (18) with parameters as in Fig. 6. The smooth curves show the projections of the model density onto the v_ϕ and v_R axes, while the histograms show the corresponding distributions of stars in the GCS.

pler expedient of using a slightly smaller value of R_d than the scale length of the disc we wish to produce.

In the middle panel of Fig. 6 the mean rotation speed declines from 225 km s^{-1} at $R = 1 \text{ kpc}$ to $\sim 200 \text{ km s}^{-1}$ at $R = 5 \text{ kpc}$ before slowly rising to 210 km s^{-1} at $R = 10 \text{ kpc}$. The bottom panel shows that the radial velocity dispersion declines throughout the disc as expected, being $\sim 34 \text{ km s}^{-1}$ at R_0 .

Fig. 7 compares the distributions of v_ϕ and v_R velocities predicted by the pseudo-isothermal DF with the corresponding distributions of GCS stars with heliocentric velocities converted to v_ϕ and v_R assuming that the circular speed is 220 km s^{-1} and the Sun’s velocity is $v_R = -10 \text{ km s}^{-1}$, $v_\phi = v_c + 5.2 \text{ km s}^{-1}$ (Dehnen & Binney 1998, hereafter DB98). The theoretical and observed distributions in v_R are satisfyingly similar, but the theoretical v_ϕ distribution lies above the observed distribution at small v_ϕ and well below it at $v_\phi \sim 200 \text{ km s}^{-1}$. We return to this issue below.

As discussed in Section 2.1, realistically we must consider the thin disc to be a superposition of pseudo-isothermal cohorts of different ages and chemical compositions. The temperature of the pseudo-isothermal DF (18) is set by the parameter σ_{r0} through equation (17). By analogy with equation (10), we should make σ_r age dependent by adding to the right side of this equation the appropriate function of τ . Then σ_r is given by

$$\sigma_r(L_z, \tau) = \sigma_{r0} \left(\frac{\tau + \tau_1}{\tau_m + \tau_1} \right)^\beta e^{q(R_0 - R_c)/R_d}. \quad (22)$$

With $\sigma_r(L_z, \tau)$ thus defined, it is natural to consider the thin-disc DF

$$\bar{f}(J_r, L_z) = \frac{\int_0^{\tau_m} d\tau e^{\tau/t_0} f_{\sigma_r}(J_r, L_z)}{t_0(e^{\tau_m/t_0} - 1)}. \quad (23)$$

where f_{σ_r} is defined by equation (18) with $\sigma_r(L_z, \tau)$ now obtained from equation (22). The DF $\bar{f}(J_r, L_z)$ correctly yields values of observables averaged through the thickness of the disc. In the case of an external galaxy such averaged observables are of interest, but samples of Milky-Way stars rarely if ever provide a sample that is unbiased in z . In particular, stars with large J_z spend little time near the Sun so samples of local stars are biased against them. Since a star with large J_z is likely to be old, it is likely to have large J_r also. Hence samples of local stars are biased towards small J_r and the DF (23) cannot be used to predict the properties of solar-neighbourhood stars, or indeed stars at that lie within any restricted range in z . Instead we must use the full thin-disc DF.

3 FULL DF

Putting together the planar and vertical parts of the DF for the thin disc introduced above, we have

$$f_{\text{thn}}(J_r, J_z, L_z) = \frac{\int_0^{\tau_m} d\tau e^{\tau/t_0} f_{\sigma_r}(J_r, L_z) f_{\sigma_z}(J_z)}{t_0(e^{\tau_m/t_0} - 1)}, \quad (24)$$

where f_{σ_r} is defined by equations (18) and (22), and f_{σ_z} is defined by equation (7) but with Ω_z and σ_z now functions of L_z through R_c . By analogy with equation (22) we have

$$\sigma_z(L_z, \tau) = \sigma_{z0} \left(\frac{\tau + \tau_1}{\tau_m + \tau_1} \right)^\beta e^{q(R_0 - R_c)/R_d}. \quad (25)$$

An orbit’s vertical frequency Ω_z is a function of all three actions, J_r , J_z and L_z . However, the Jeans theorem assures us that the DF remains a solution of the collisionless Boltzmann equation if in Ω_z we set $J_r = 0$. Restricting the J_r -dependence of the DF in this way makes the DF easier to work with and is consistent with the work of Section 2.1, which was restricted to orbits that have $J_r = 0$ (“shell orbits”). Therefore in the following we do this.

Our final thin-disc DF (24) is characterised by eight free parameters, L_0 , R_d , q , σ_{r0} , σ_{z0} , β , τ_1 and τ_m .

3.1 Thick disc DF

At the end of Section 2.1 we saw that the observed vertical density profile at the Sun can be reproduced by adding to the composite DF of the thin disc a pseudo-isothermal component with $\sigma_{z0} = 38 \text{ km s}^{-1}$ that contains 20 percent of the mass. This result suggests that we add to the DF (24) of the thin disc the thick-disc DF

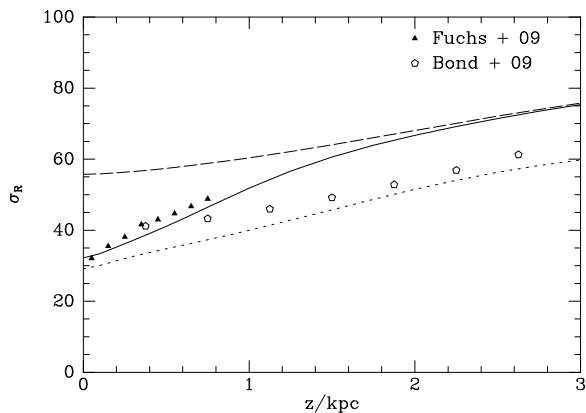
$$f_{\text{thk}}(J_r, J_z, L_z) = f_{\sigma_r}(J_r, L_z) f_{\sigma_z}(J_z), \quad (26)$$

where f_{σ_r} and f_{σ_z} are defined by equations (18) and (7) above with σ_r and σ_z given by

$$\begin{aligned} \sigma_r(L_z) &= \sigma_{r0} e^{q(R_0 - R_c)/R_d} \\ \sigma_z(L_z) &= \sigma_{z0} e^{q(R_0 - R_c)/R_d}, \end{aligned} \quad (27)$$

Table 1. Parameters of the standard DF (upper section) and values used by Bensby et al. (2003) (lower section)

	Thin disc	Thick disc
L_0	10 km s ⁻¹	10 km s ⁻¹
R_d	2.25 kpc	2.3 kpc
q	0.45	0.45
σ_{r0}	33.5 km s ⁻¹	60 km s ⁻¹
σ_{z0}	19 km s ⁻¹	32 km s ⁻¹
k_{thk}	-	0.24
β	0.33	-
t_0	8 Gyr	-
τ_1	110 Myr	-
τ_m	10 Gyr	-
<hr/>		
σ_U	35 km s ⁻¹	67 km s ⁻¹
σ_V	20 km s ⁻¹	38 km s ⁻¹
σ_W	16 km s ⁻¹	35 km s ⁻¹
V_a	15 km s ⁻¹	46 km s ⁻¹

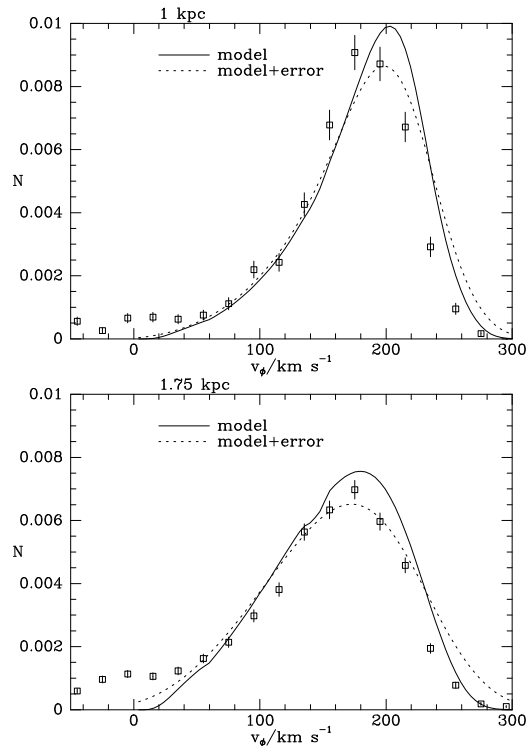

Figure 8. The full curve shows the radial velocity dispersion in the standard model. The dotted and dashed lines show the dispersions in the thin- and thick-disc components, respectively. The triangles show estimates of σ_R for metal-poor M dwarfs from Fuchs et al. (2009), while the open pentagons show the analytic fit to $\sigma_R(z)$ given by Bond et al. (2009)

and in equation (18) we use (cf eq. 21)

$$\Sigma = k_{\text{thk}} e^{(R_0 - R_c)/R_d}. \quad (28)$$

Here k_{thk} is the ratio of thick to thin-disc stars in the solar cylinder. In principle this thick-disc DF introduces a further six parameters: L_0 , R_d , q , σ_{r0} , σ_{z0} and k_{thk} . Table 1 lists all the parameters of the standard DF. We have not explored the option of using a different value of L_0 for each disc because this parameter has a negligible impact on comparisons with local data.

The choice of σ_{z0} and k_{thk} for the thick disc is straightforwardly made by the requirement that the vertical density profile match the data of Gilmore & Reid (1983). The choice of R_d , q and σ_{r0} for the thick disc is more problematic. Clearly these parameters should be constrained by the radial density and kinematics of the disc at $z > 1$ kpc, where the thick disc is dominant. The strongest constraints are provided by the SDSS. Juric et al. (2008) found the scalelength of the thick disc to be similar to that of the thin disc. Bond et al. (2009) give an analytic fit to the dependence of σ_R on


Figure 9. Distributions of v_ϕ velocities 1 kpc (top panel) and 1.75 kpc (lower panel) above the plane. The data points are from Ivezić et al. (2008) for stars with $0.8 \text{ kpc} < z < 1.2 \text{ kpc}$ (upper panel) and $1.5 \text{ kpc} < z < 2 \text{ kpc}$ (lower panel). The full curves show the model distributions at $z = 1 \text{ kpc}$ and 1.75 kpc . The dashed curves show the result of convolving this distributions with the measurement errors of Ivezić et al.

z out to $z \simeq 4 \text{ kpc}$, and Fuchs et al. (2009) give several values of σ_R at $z \leq 800 \text{ pc}$. Finally Ivezić et al. (2008) provide distributions in v_ϕ in several ranges of z . Figs 8 and 9 show these data.

Although the data sets are less clearly inconsistent than they are in Fig. 3, the data from Fuchs et al. clearly show a significantly steeper gradient than those from Bond et al. In the model $\sigma_R(z)$ has a slope intermediate between these values, and agrees with the data at $z \lesssim 1 \text{ kpc}$. At greater heights it lies above the Bond et al. data, just as the model curve does in Fig. 3.

The model's predictions for the distribution in v_ϕ at $z = 1 \text{ kpc}$ and $z = 1.75 \text{ kpc}$ are shown in Fig. 9 together with data points from Ivezić et al. (2008) the heliocentric data of Ivezić et al. (2008) have been converted to galactocentric velocities assuming $v_\phi(\odot) = 225.2 \text{ km s}^{-1}$, which arises because in our adopted potential the circular speed is 220 km s^{-1} and the peculiar V velocity of the Sun is 5.2 km s^{-1} (Dehnen & Binney 1998). The full curves are the true model velocity distributions, and the dotted curves show the result of convolving these distributions with the errors reported by Ivezić et al., which are 19.5 km s^{-1} at $z = 1 \text{ kpc}$ and 31.5 km s^{-1} at $z = 1.75 \text{ kpc}$.

The model curves fall below the data at $v_\phi \lesssim 50 \text{ km s}^{-1}$ because in this region halo stars dominate the data points and the model is for the disc alone. Elsewhere the dotted curves provide a moderate fit to the data points. The fit in the upper panel would be improved by moving the data

points a few km s^{-1} to the right, which would be the effect of the upward revision of the Sun's peculiar velocity advocated below. The model curves are slightly too broad. Reducing the parameter σ_r in the thick-disc DF makes them narrower, but this change also shifts the model curves still further to the right, and thus makes the overall fit less good. The distributions can also be made narrower by either increasing the thick-disc scalelength R_d or by decreasing q . However either change decreases the importance of stars at apocentre (which have angular momentum $L_z < L_z(\odot)$) relative to those at pericentre and thus exacerbates the predicted excess of stars at large v_ϕ . Extensive experimentation suggests that the fits shown in Fig. 9 cannot be significantly improved upon with a DF of the form (26).

Because they are extracted from proper-motion data, the observational distributions in Fig. 9 are sensitive to the photometric distances employed. A possible resolution of the conflict in the lower panel of Fig. 9 between the model and data is that the distances employed are slightly too small: using larger distances would increase heliocentric velocities and thus cause the observational points to move away from the Sun's assumed velocity, $v_\phi = 225.2 \text{ km s}^{-1}$. Another possible resolution of the conflict between data and models in Fig. 9 is the increasing inaccuracy of the assumption of adiabatic invariance of the vertical motion as random motions become more important. In a future publication this possibility will be examined with models based on orbital tori.

3.2 The standard DF and the solar neighbourhood

Fig. 10 shows prediction of the standard DF for the structure of the solar neighbourhood. Full curves are for the whole disc and dashed curves show the contribution of the thin disc. The upper panels show for stars seen in the plane the distributions in v_ϕ and v_R after integrating over the other two velocity components. Comparison of these panels with the panels of Fig. 7 is instructive. The distribution of v_R velocities is in reasonable agreement with the data, while the distribution of v_ϕ velocities of Fig. 10 agrees with the data better than the distribution in v_ϕ in Fig. 7. Two factors contribute to the improved fit to the v_ϕ velocities. First introducing a sum of pseudo-isothermals enhances both the core and the wings of the distribution – this effect is apparent in the distributions of v_R velocities. More significantly, including vertical motion suppresses the v_ϕ distribution at low v_ϕ because this wing of the distribution is populated by stars with small values of R_c that reach the solar neighbourhood because they have large random velocities. On account of those large velocities, they have low probabilities of being found close enough to the plane to be included in the GCS. These stars are most likely to be observed near apocentre, when they have low values of v_R , so depressing the contribution to the GCS of such stars does not suppress the wings of the distribution of v_R velocities.

The plots shown in Fig. 10 are obtained by setting the function $\Sigma(R_c)$ for the thin disc that appears in the DF to the same exponential with scale length 2.25 kpc that was used to obtain Figs 6 and 7. The use of 2.25 kpc in $\Sigma(R_c)$ is important not only to ensure that the disc's surface density is approximately exponential with the larger scale length 2.5 kpc, but also to ensure that the predicted distribution of

v_ϕ velocities agrees with the GCS data: when Σ has scale length 2.5 kpc, the predicted distribution falls off too slowly at $v_\phi > v_c$.

The model v_ϕ distribution deviates from the data in two respects: it lacks the pronounced peak in the data centred on $v_\phi = 205 \text{ km s}^{-1}$, and it extends too far on the high-velocity wing. The first shortcoming undoubtedly reflects the axisymmetry of the model and is discussed below. The second shortcoming, which is also evident in the fits to the data of Ivezić et al. (2008) for the thick disc (Fig. 9), is more interesting. It can be moderated by increasing the parameter q of equation (22). This parameter controls the radial gradient of the thin disc's velocity dispersion, and a rapid decrease in the amplitude of epicycle motions at $R_c > R_0$ limits the number of stars with large angular momentum that can reach the Sun and thus depopulates the high- v_ϕ wing. However, an increase in q boosts the model profile at low v_ϕ , so the overall agreement with the data is not improved unless the parameter σ_{r0} of equation (22) is simultaneously decreased, and such a decrease leads to the model v_R distribution being narrower than the data warrant.

Oort's relation e.g., BT08 eq. (4.317)

$$\frac{\sigma_\phi^2}{\sigma_R^2} = \frac{-B}{A-B} \quad (29)$$

implies that the width of the model v_ϕ distribution can be decreased relative to that of the v_R distribution by changing from a flat to a falling circular-speed curve. However, one finds that the relative narrowing of the v_ϕ distribution that is produced by adopting the power-law potential (19) with $\alpha = -0.2$ produces a negligible improvement on the fit for constant circular speed shown in Fig. 10.

The bottom left panel of Fig. 10 shows that the overall DF provides an excellent fit to the vertical density profile from Gilmore & Reid (1983), and that the vertical profile of the thin disc is extremely close to exponential. The latter result appears to be fortuitous in that it involves a subtle interplay between the non-trivial vertical force law and the number of stars with large random velocities that visit the solar neighbourhood from significantly nearer the Galactic centre.

The bottom right panel of Fig. 10 shows that in both the thin and thick discs the mean rotation speed declines with distance from the plane. In the plane the thin disc rotates faster than the thick disc, as one naively expects. However, the rotation rate of the thin disc declines faster with z than that of the thick disc. The slower decline in the thick disc arises because we have set $R_d = 2.3 \text{ kpc}$ in the function $\Sigma(R_c) = e^{-R_c/R_d}$ for the thick disc – with $R_d = 2.25 \text{ kpc}$ for both discs the thick disc rotates $\sim 15 \text{ km s}^{-1}$ slower than the thin disc at all values of z . We have chosen $R_d = 2.3 \text{ kpc}$ for the thick disc to obtain a better fit to the long-dashed curve in the lower right panel of Fig. 10, which is an analytic fit to the mean rotation rate extracted from the proper motions of SDSS stars by Ivezić et al. (2008). The dependence of the rotation rate on R_d is consistent with the Stromberg equation

$$v_a = \frac{\sigma_R^2}{2v_c} \left[\frac{\sigma_\phi^2}{\sigma_R^2} - 1 - \frac{\partial \ln(\nu \sigma_R^2)}{\partial \ln R} - \frac{R}{\sigma_R^2} \frac{\partial \sigma_{Rz}^2}{\partial z} \right]. \quad (30)$$

For our preferred DF the asymmetric drift of the thick disc increases from only 20 km s^{-1} at $z = 0$ to 90 km s^{-1} at

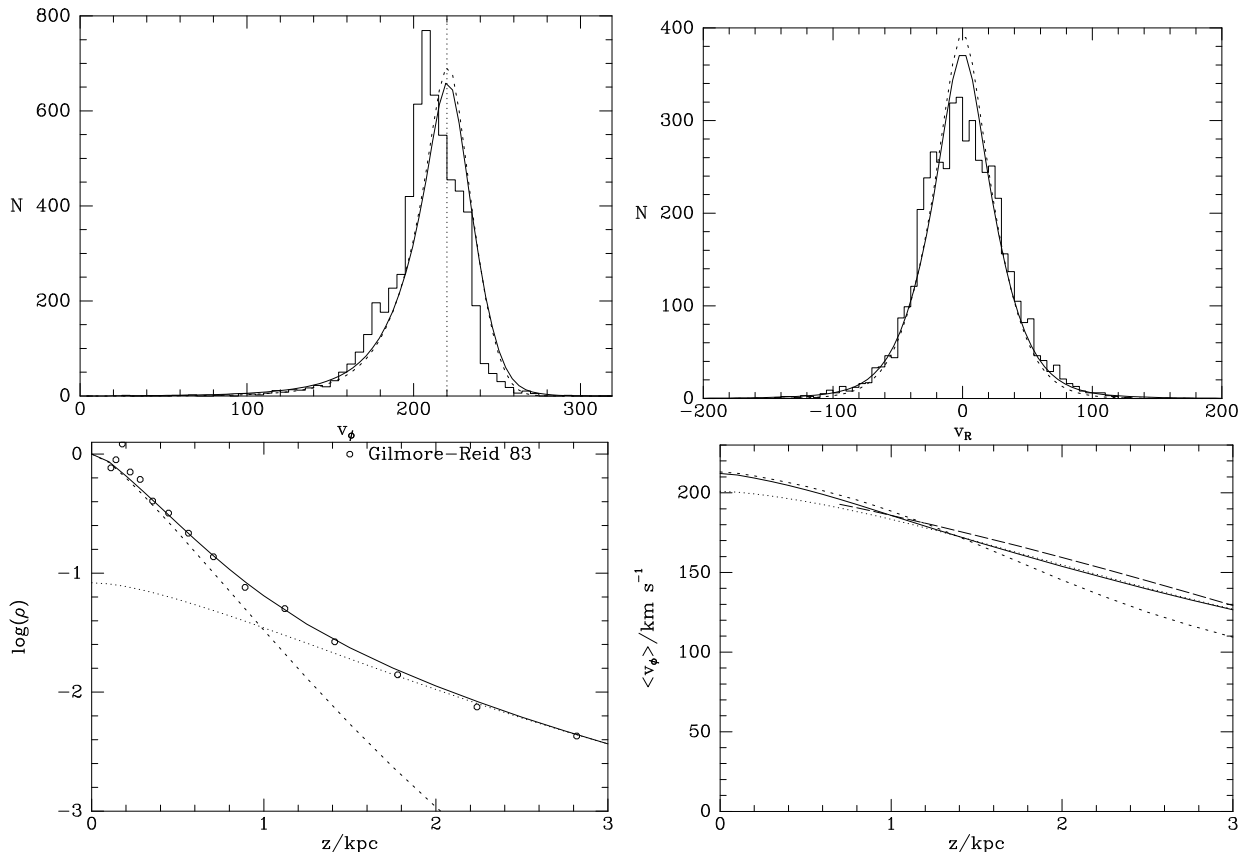


Figure 10. Structure at the solar radius predicted by the standard DF (eqs. 24 and 26). Full curves are for the entire disc while dashed curves show the contribution of the thin disc. The upper panels show velocity distributions for $z = 0$ marginalised over the other velocity components. The vertical dotted line marks the local circular speed. In the lower panels dotted curves show the contributions of the thick disc. In the bottom-right panel the long-dashed line is the empirical fitting function of Ivezić et al. (2008). The values of the DF’s parameters are given in Table 1.

$z = 3$ kpc, consistent with the values $30 - 50 \text{ km s}^{-1}$ usually reported by observers (e.g. Edvardsson et al. 1993; Gilmore et al. 1989).

Fig. 11 compares the observed density of stars in the plane of velocities (U, V) with respect to the LSR¹ (top panel) to that predicted by the standard DF (bottom). The dynamic range in density that can be sampled with the GCS stars is limited, so only a portion of the standard DF’s predictions for the (U, V) plane is tested. Moreover, the limited number of GCS stars leads to the steepness of density gradients being underestimated, for example around $(U, V) = (0, 40) \text{ km s}^{-1}$.

Near $(U, V) = (0, 0)$, the observational diagram shows density enhancements, or “streams”, that are not bounded by the roughly ellipsoidal surfaces in velocity space on which actions are constant. Consequently, by Jeans’ theorem, the presence of streams indicates that either the Galaxy’s potential is not axisymmetric, or the Galaxy is not in a steady state – no DF that is a function of actions only can reproduce these streams, although one hopes to be able to re-

produce them by perturbing such a DF using Hamiltonian perturbation theory. The streams account for much of the disagreement between the theoretical and observed velocity distributions in Fig. 10. In particular they account for the peak in the observed v_ϕ distribution lying $\sim 15 \text{ km s}^{-1}$ below the circular speed.

3.3 The solar motion

We have seen that the DF has difficulty simultaneously fitting the observed distributions in v_R and v_ϕ of the GCS stars (top panels of Fig. 10). A related problem was encountered in the fit to the proper motions of thick-disc stars (Fig. 9). The agreement between theory and data in both figures would be improved by shifting the observed v_ϕ distribution to the right. Such a shift would correspond to increasing the Sun’s peculiar velocity by a few kilometers per second.

Although such a shift significantly exceeds the formal error of 0.6 km s^{-1} on V_\odot given by DB98, we should not lightly dismiss the possibility that V_\odot has been underestimated. The value given by DB98 was obtained by extrapolating to zero velocity dispersion a plot of V velocity versus squared velocity dispersion S^2 for stars grouped by colour such as that shown in Fig. 12. Stromberg’s equation (30) suggests that this relation will be linear if the square bracket

¹ We follow BT08 (p. 12) in defining the LSR to be $v_R = v_z = 0$ and $v_\phi = v_c(R_0)$. The LSR is sometimes taken to be the speed of a closed orbit through R_0 . In the presence of ephemeral spiral structure this second definition is probably not useful.

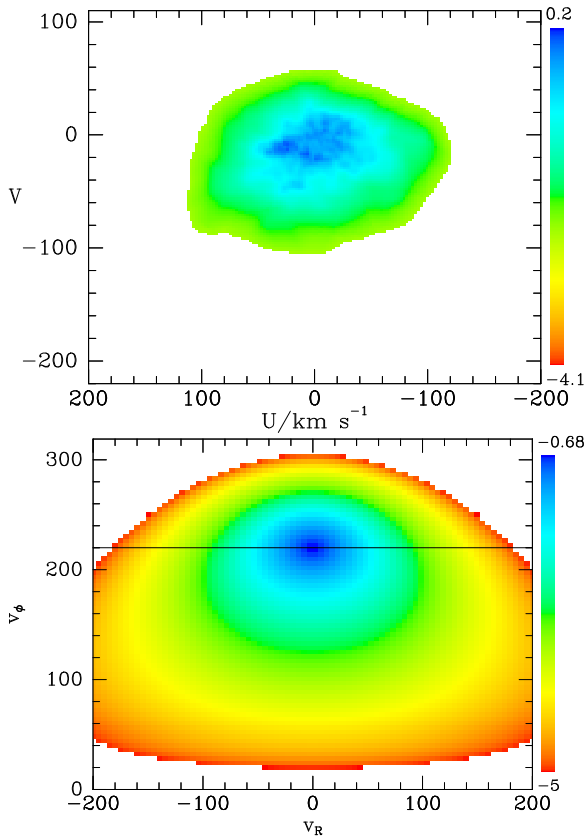


Figure 11. The density of GCS stars in the (U, V) plane (upper panel) and that predicted by the standard DF (lower panel). Colours indicate \log_{10} of the stellar density and the horizontal line is at the circular speed. The upper plot was obtained by applying the FiEstas algorithm of Ascasibar & Binney (2005) to the GCS data and setting the density to zero if there was no star within 25 km s^{-1} of a point.

is constant, and Fig. 12 shows that the Hipparcos data are consistent with this expectation if the groups with the lowest velocity dispersions (shown in red) are discounted. However, Stromberg’s equation is obtained under the assumption that the Galactic potential is axisymmetric, so in the limit of vanishing velocity dispersion, stars move on circular orbits. In reality the potential has a non-axisymmetric component of amplitude $\sim 7 \text{ km s}^{-1}$, which manifests itself, inter alia, by causing a plot of terminal velocity versus Galactic longitude to undulate at this level (e.g. Malhotra 1995; Binney & Merrifield 1998, Fig. 9.16). Given the non-axisymmetric component of the potential, $\lim_{\sigma \rightarrow 0} \langle V \rangle$ can differ from the velocity of circular motion by of order the amplitude $\sim 7 \text{ km s}^{-1}$ of the non-axisymmetric component.

As Olling & Dehnen (2003) pointed out in their determination of the Oort constants, the larger the velocity dispersion a population has, the less it is likely to be affected by non-axisymmetric forces associated with spiral structure. The non-axisymmetric potential of the Galaxy’s bar is thought to be responsible for the “Hercules stream”, an overdensity of stars in velocity space around $v_\phi = v_c - 50 \text{ km s}^{-1}$, but there is no evidence that it significantly perturbs the velocity distribution at $v_\phi \gtrsim v_c$, where the standard model conflicts with the data. Consequently, Fig. 10 offers an op-

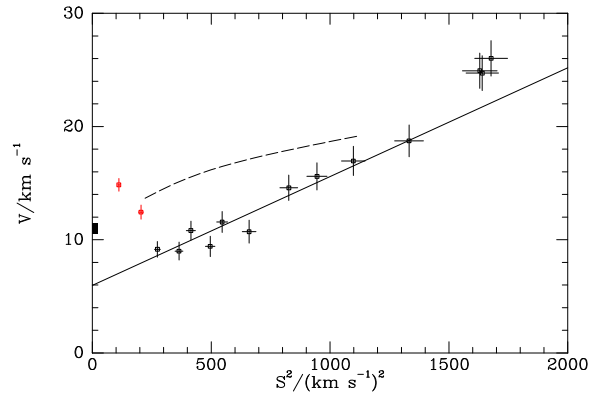


Figure 12. The data points show, for each group of 1000 main-sequence stars ordered by colour, the solar motion versus the group’s squared velocity dispersion in the plane of the sky. The points are based on the proper motions obtained by van Leeuwen (2007) from a reanalysis of the Hipparcos telemetry for samples of stars defined by Aumer & Binney (2009). The straight line is the least-squares fit to the black data points, which has y intercept at 5.05 km s^{-1} . The black rectangle on the y axis shows the proposed solar motion $V_\odot = 11 \text{ km s}^{-1}$. The dashed line shows the solar motions predicted by model DFs for populations ranging in age from 1 to 11 Gyr under the assumption that $V_\odot = 11 \text{ km s}^{-1}$ and $S^2 \simeq (1.2\sigma_R)^2$ (DB98).

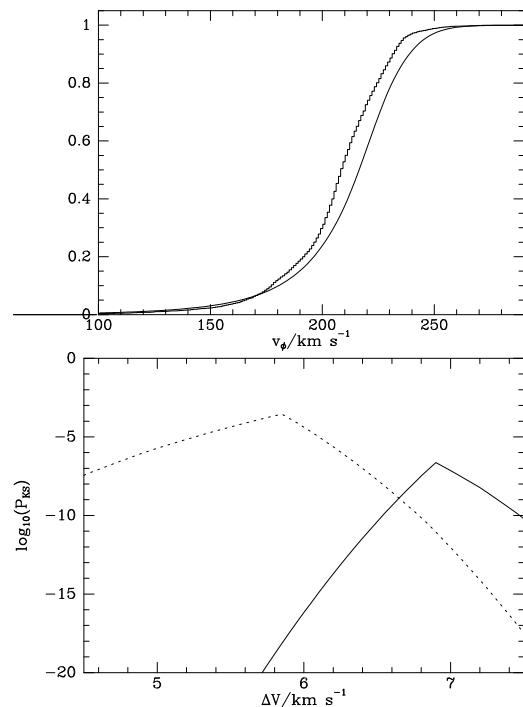


Figure 13. Upper panel: the cumulative distributions of stars with v_ϕ smaller than the given value for the GCS data (jagged curve) that the standard DF under the assumption $V_\odot = 5.2 \text{ km s}^{-1}$ from DB98. Lower panel: the full curve shows the Kolmogorov–Smirnov probability that the distribution of V velocities of GCS stars is drawn from a model distribution as a function of the amount ΔV added to 5.2 km s^{-1} . Dotted curve: the same but after randomly redistributing those observed stars that have velocities with respect to the conventional LSR in the range $(-20, 10) \text{ km s}^{-1}$.

portunity to determine V_\odot that is at least as valid as the traditional route using Stromberg's equation.

The jagged curve in the upper panel of Fig. 13 shows the cumulative distribution in v_ϕ of the GCS stars under the assumption that $v_c(R_0) = 220 \text{ km s}^{-1}$ and $V_\odot = 5.2 \text{ km s}^{-1}$. The smooth curve shows the cumulative distribution of the model shown in Fig. 10. The need to shift the distribution of GCS stars to the right is evident.

The full curve in the lower panel of Fig. 13 shows the Kolmogorov–Smirnov probability P_{KS} that the distribution of V velocities of GCS stars is drawn from the model shown in Fig. 10 as a function of the amount ΔV added to the solar motion given in DB98. For all choices of ΔV , P_{KS} is small, largely due to the impact of streams on the data for $-20 \text{ km s}^{-1} \lesssim V_{\text{LSR}} \lesssim 10 \text{ km s}^{-1}$. The impact of streams on P_{KS} can be reduced by randomly redistributing stars within this range of V_{LSR} . The dotted curve in Fig. 13 shows the dependence of P_{KS} on ΔV when the randomised sample is compared to the model. The peak in P_{KS} rises by three orders of magnitude and shifts from $\Delta V = 6.9 \text{ km s}^{-1}$ to 5.8 km s^{-1} .

Thus the stars that should be least affected by spiral structure suggest that DB98 underestimated V_\odot by $\Delta V = 5.8 \text{ km s}^{-1}$, so the true solar motion is $V_\odot = 11 \text{ km s}^{-1}$. The systematic error $\sim 1 \text{ km s}^{-1}$ on this value is clearly much greater than the formal error reported by DB98. In Fig. 12 the black rectangle marks this revised solar motion.

It is interesting to test the extent to which Stromberg's equation is verified by pseudo-isothermal DFs for main-sequence stars of a given colour. The dashed curve in Fig. 12 shows the relation between $S^2 \simeq (1.2\sigma_R)^2$ (DB98) and V_a that one obtains by calculating these quantities for a DF of the form (24) with τ_m increasing from 1 to 11 Gyr; over this age range σ_R increases from 12.4 to 28 km s^{-1} . The dashed curve is plotted on the assumption that the solar motion is $V_\odot = 11 \text{ km s}^{-1}$, as marked by the black rectangle. At low S^2 the slope of the dashed curve is similar to the slope of the observational relation, but the slope flattens perceptibly with increasing S^2 . This flattening implies that the square bracket in Stromberg equation (30) diminishes with increasing velocity dispersion. There is no evident reason why this bracket should be constant.

It is not inconceivable that spiral structure and/or the bar have shifted the observational points with S^2 in the range (250, 700) downwards from a relation that runs from the black square, between the red points and on to just above the points at $S^2 > 1200$. Moreover, a proponent of the conventional value of V_\odot should worry that if the dashed curve were moved down to start at that value of V_\odot , it would lie below nearly all the data points. We conclude that although we cannot confidently recommend an upward revision of V_\odot , considerable caution should be exercised in the use of the conventional value and more work is needed on the effect that spiral structure has on the local velocity space.

Analysis of the space velocities of 18 maser sources for which trigonometric parallaxes are available (Reid et al. 2009) provides tentative support for V_\odot being revised upwards to 11 km s^{-1} (McMillan & Binney 2009).

The values of V_\odot , the proper motion of Sgr A*, $6.38 \pm 0.04 \text{ mas s}^{-1}$ (Reid & Brunthaler 2004), and the distance to Sgr, A*, $8.33 \pm 0.31 \text{ kpc}$ (Gillessen et al. 2009), determine the local circular speed $v_c(R_0) = R_0\mu_{A*} - V_\odot = (251 \pm 12 -$

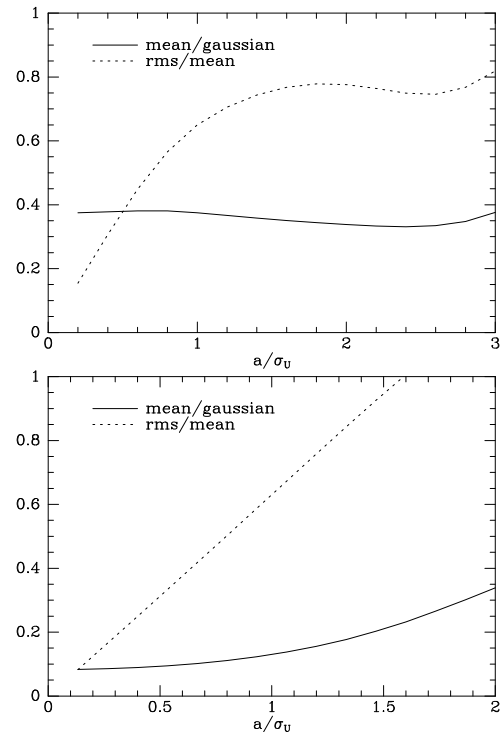


Figure 14. Full curves: the mean value of the thin-disc DF (upper panel) and the thick-disc DF (lower panel) over an ellipsoid in velocity space on which the model DF (31) is constant, divided by that constant value. Dotted curves: the rms variation over an ellipsoid in the model DF divided by the mean value on the ellipsoid. The x axis gives the semi-major axis of the ellipsoid in multiples of σ_U .

V_\odot) km s^{-1} . Flynn et al. (2006) estimate the absolute I-band luminosity of the Galaxy to be $M_I = -22.3$. At this absolute magnitude the ridge-line of the I-band Tully–Fisher relation (Dale et al. 1999) gives a circular speed of only 190 km s^{-1} ; 251 km s^{-1} lies 2.6σ from the ridge line. Thus the likelihood of the Galaxy in the context of the Tully–Fisher relation is small but increases rapidly with V_\odot , and this fact provides further support for an upward revision of V_\odot .

3.4 Distinguishing the thin and thick discs

Studies of the chemistry of the thick disc depend heavily on identifying nearby, bright stars that belong to the thick disc as targets of medium-dispersion spectroscopy (Fuhrmann 1998; Bensby et al. 2003; Venn et al. 2004; Bensby et al. 2005; Gilli et al. 2006; Reddy et al. 2006). A popular strategy for identifying target stars is to assume ellipsoidal velocity distributions for each disc of the form (Bensby et al. 2003)

$$f(U, V, W) \propto \exp\left(-\frac{U^2}{2\sigma_U^2} - \frac{(V - V_a)^2}{2\sigma_V^2} - \frac{W^2}{2\sigma_W^2}\right), \quad (31)$$

where (U, V, W) are velocity components with respect to the LSR, and each component is assigned assumed values of $\sigma_U, \sigma_V, \sigma_W$ and the rotational lag V_a . A given star is assigned to the population for which it gives the largest value of the DF that follows from equation (31) and assumed fractions of local stars that belong to each population.

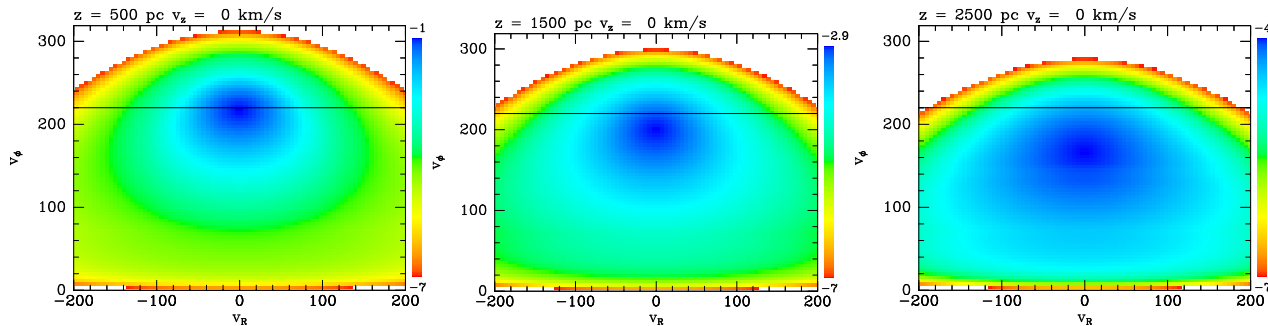


Figure 15. Distributions in the (v_R, v_ϕ) plane for $v_z = 0$ at three distances from the plane: 0.5 kpc (left), 1.5 kpc (centre) and 2.5 kpc. Exactly these distributions are predicted at $z = 0$ and $v_z = 30, 67$ and 97 km s^{-1} .

The idea behind equation (31) is that, for appropriate parameters, f provides a useful approximation to the DFs of the two discs. Here we investigate the quality of this approximation by comparing f with the thin- and thick-disc components of the standard DF when the parameters in f take the values used by Bensby et al. (2003), which are given in Table 1. Fig. 14 quantifies the quality of the approximation provided by f by reporting the fractional RMS variation in the appropriate component of the standard DF over each ellipsoidal surface in velocity space on which f is constant (dotted curves) – ideally this would vanish. The full curves show the mean value of the DF over an ellipsoid of constant f , divided by the value of f on that ellipsoid – since the normalisation of f is arbitrary, the full lines in Fig. 14 may be shifted up or down at will, but must be horizontal if f it to provide a useful approximation to the relevant component of the standard DF.

The upper panel of Fig. 14 is for the thin disc and the lower panel for the thick disc. Since the full curve in the upper panel is approximately horizontal, we conclude that f decreases from small to large ellipsoids in the same way that our model thin-disc DF does. However, from the fact that the dotted curve lies above 0.7 for $a > \sigma_U$, we conclude that the model DF varies by of order itself over the larger velocity ellipsoids of the thin disc. Thus f is a useful but not very accurate approximation to the model DF for the thin disc.

The lower panel of Fig. 14 implies that f provides a very poor approximation to our model thick-disc DF: not only does the full curve rise by more than a factor of 4 as a increases to $2\sigma_U$, but the essentially linear rise of the dotted curve implies that the model DF varies strongly over ellipsoids of constant f . What prevents f providing a good approximation to the DF is the continuous increase in the asymmetric drift as the numerical value of the DF decreases. This increase is apparent in the downward motion of isodensity contours in Fig. 11 and drives the fall in $\langle v_\phi \rangle$ with z in the bottom right panel of Fig. 10. In particular, at $z = 0$ the density of stars in velocity space peaks close to the circular speed in the thick disc as in the thin. This fact conflicts with the structure of equation (31).

3.5 Local and in-situ samples

The standard DF predicts that the distribution of stars in the (v_R, v_ϕ) plane at height z and $v_z = 0$ is identical to the

(v_R, v_ϕ) distribution of stars at any other height $z' < z$ and velocity $v'_z = \{2[\Phi_z(z) - \Phi_z(z')]\}^{1/2}$. Moreover, a sample of stars observed at some distance z from the plane will be heavily weighted towards stars whose vertical motions have turning points there. So there should be a close correspondence between local stars with a particular value of v_z and samples of stars at a given value of z . Since the SDSS and its successors provide photometric distances and proper motions for millions of stars that lie $\gtrsim 1$ kpc from the plane, and the GCS catalogue provides space velocities for over ten thousand nearby stars, this correspondence can be tested in some detail. Fig. 15 shows some sample (v_R, v_ϕ) distributions.

4 CONCLUSIONS

We have explored the ability of distribution functions to provide models of the thin and thick discs of the Milky Way. Our DFs are analytic functions of the actions of orbits, which ensures that there is an intuitive relation between the observable properties of the population a DF describes and the functional form of the DF, and a meaningful way to compare models that use different gravitational potentials. In this paper we have used expressions for the actions that are only approximate, and imply that a star’s vertical motion is adiabatically invariant during the star’s motion parallel to the plane. In a forthcoming paper (McMillan et al., in preparation) orbital tori will be used to eliminate this approximation, and thus quantify its validity.

We have shown that the vertical density profile and kinematics of the disc are accurately modelled by the extremely simple DF (9). However, we rejected this DF because it is essential to be able to break the DF for the thin disc down at least into contributions from stars of various ages, and ideally into contributions from ranges in both age and metallicity. That is, we must recognise that the Galaxy is built up of innumerable stellar populations of various ages and metallicities, and each population has its own DF. In this paper we have only begun to explore the resulting complexity by ascribing a single DF to the thick disc and modelling the thin disc as a superposition of DFs for stars of different ages. In reality both discs are chemically inhomogeneous and we should assign a distinct DF to the stars born at each time with each chemical composition (e.g. Schönrich & Binney 2009). Hence the DFs presented in this paper should be

considered building blocks from which more elaborate DFs may be in due course constructed.

Our most basic building block is a “pseudo-isothermal” population of stars. Fig. 1 shows that the vertical distributions of young stellar populations is well modelled by a pseudo-isothermal population. The density of a pseudo-isothermal population does not decline exponentially with z , but Figs. 4 and 10 show that, remarkably, the composite population produced by stochastic acceleration of stars does have an exponentially decreasing density profile. An excellent fit to the observed density profile of the entire disc is obtained when a pseudo-isothermal thick disc is added to the composite thin disc. The dispersion in v_z of thin-disc stars increases from 17.4 km s^{-1} in the plane to 33 km s^{-1} at 2.5 kpc , while that of the thick-disc stars increases from $\sim 35 \text{ km s}^{-1}$ in the plane to $\sim 48 \text{ km s}^{-1}$ at 2.5 kpc . The thick disc contributes to the solar cylinder 24 per cent of the luminosity contributed by the thin disc, or 19.4 per cent of the total luminosity of the disc.

Even though we are assuming that the dynamical coupling between motions in and perpendicular to the plane is weak, two features of our DFs lead to strong correlations between distributions in v_R and v_z . One feature is the fact that random velocities must increase as one moves inwards, and the other is the simultaneous increases in σ_R and σ_z that are driven by stochastic acceleration of a coeval population. Comparison of Figs. 7 and 10 show that, on account of this correlation, the distribution of local stars in the (v_R, v_ϕ) plane is atypical of the stellar population of the whole solar cylinder in just such a way that our composite disc DF can simultaneously provide reasonable matches to the very different shapes of the distributions of GCS stars in v_R and v_ϕ . The widths of the model distributions in v_R and v_ϕ are controlled by a single parameter, σ_{r0} . The shape of the v_R distribution is predetermined by our choice of the DFs functional form. The value of the parameter R_d provides limited control of the shape of the v_ϕ distribution and we obtain the best fit to the observed distribution when this parameter is chosen such that the disc’s surface density declines roughly exponentially with scale length 2.5 kpc , which happens to agree with the scale length inferred from near-IR star counts by Robin et al. (2003).

In principle the DF of the thick disc should be tightly constrained by the dependence on z of the velocity dispersions σ_R and σ_z . These dependencies have recently been determined for SDSS stars by two groups. Unfortunately, their results seem to be incompatible and the reasons for the conflict are unknown.

The standard model provides an excellent fit to the seminal work of Kuijken & Gilmore, perhaps because the gravitational potential in which the DF is evaluated was partly fitted to that work. Some of the difficulties encountered here with fitting newer data may arise from inaccuracy of the potential used. A worthwhile exercise would be to fit data from the GCS, RAVE and SDSS surveys to models that combined DFs of the type presented here with and a multi-parameter gravitational potential: by simultaneously fitting the parameters in both the DF and the potential, one should be able to obtain reasonable fits to the data, providing the latter have been purged of such evident inconsistencies as those seen in Fig. 3. Data from more than one survey would probably have to be used since SDSS stars are too faint to constrain the

thin disc tightly, although the RAVE survey, which certainly probes the thick disc effectively, may include enough nearby stars to make the Hipparcos-based GCS survey obsolete.

The model fit to the v_ϕ distribution of GCS stars is far from perfect. Some of the disagreement arises because, as is well known, the Galactic bar and spiral arms give rise to features (“star streams”) in the local velocity distribution that are inconsistent with the Galaxy being axisymmetric and in a steady state, as our models assume. Our favoured model v_ϕ distribution would fit the data better if the conventional value of the solar motion V_\odot were $\sim 6 \text{ km s}^{-1}$ too low. Tentative support for such an increase in the V_\odot is provided by astrometry of stellar masers (Reid et al. 2009; McMillan & Binney 2009), and any increase would also tend to bring the Galaxy more into line with the Tully–Fisher relation between v_c and M_I for external galaxies. By systematically perturbing the velocities of all solar-neighbourhood stars, spiral structure might lead to the classical approach to the determination of V_\odot yielding an underestimate. Further work is required to explore this possibility, and at this stage we would merely stress that the systematic error in V_\odot is much larger than the formal errors given by DB98 and Aumer & Binney (2009).

In the models, the asymmetric drifts of both the thin and thick discs increase with height. A disc’s asymmetric drift is largely controlled by its parameter R_d and in the standard model the asymmetric drift of the thin disc exceeds that of the thick disc above 1 kpc because we have adopted a slightly larger value of R_d for the thick disc than for the thin disc.

A popular strategy for assigning solar-neighbourhood stars to the thin or thick disc is to find the values taken by each disc’s model DF at the star’s location. The model DFs used are perfectly ellipsoidal but we show that such DFs provide poor approximations to the thick-disc component of the standard DF, so a markedly cleaner separation of the two discs could be obtained by replacing the ellipsoidal DFs by the thin- and thick-disc components of the standard DF.

Although the observational material relating to the Galaxy has increased enormously in recent years, we have shown that much of the available data can be successfully modelled with a simple analytical DF. In a couple of aspects the data are in mild conflict with the DF, but it is at least as likely that the fault lies with the data as the DF. In the coming decade the volume and quality of the observational material available will increase dramatically. We anticipate that comparisons between each new data set and an evolving standard DF will reveal successes and failures similar to those encountered here. The successes will confirm the value of the DF as a summary of a large and inhomogeneous body of data, and the failures will lead to critical re-examination of both data and DF. Sometimes the failure will arise from a defective calibration of the data or incorrect assumptions used in its reduction, and other times it will indicate that the DF is too simplistic. Either way we will learn something new and interesting.

In this paper the DF’s parameters have been fitted to the data by eye and no attempt has been made to quantify uncertainties in parameter values. Clearly such uncertainties are important, and they could be most securely established by carrying the DF’s predictions closer to the raw observations than we have done. In future work probability dis-

tributions in colour–magnitude–proper-motion space, etc., should be predicted that can be compared with the actual star counts.

Upcoming infrared surveys, such as the VHS with Vista and APOGEE, will probe the disc at remote locations. The predictions of the standard DF for those locations will be presented shortly, after orbital tori have been introduced as the means to convert between Cartesian and angle-action variables. This upgrade will make obsolete the approximation of adiabatically invariant vertical motions used here.

ACKNOWLEDGEMENTS

I thank Michael Aumer for providing the data shown in Fig. 12 and Zeljko Ivezić for providing the data plotted in Fig. 9. The members of the Oxford dynamics group contributed valuable comments on drafts of this work. It is a pleasure to acknowledge valuable conversations with Ralph Schönrich.

REFERENCES

- Abazajian K., et al., 2009, ApJS, 182, 543-558
 Ascasibar Y., Binney J., 2005, MNRAS, 356, 872
 Aumer M., Binney J., 2009, MNRAS, in press (arXiv 0905.2512)
 Bensby T., Feltzing S., Lundström I., 2003, A&A, 410, 527
 Bensby T., Feltzing S., Lundström I., Ilyin I., 2005, A&A, 433, 185
 Binney J., 1987, in “The Galaxy”, eds. G. Gilmore & R. Carswell (Dordrecht: Reidel) p. 399
 Binney J., Merrifield M., 1998, “Galactic Astronomy”, Princeton University Press, Princeton
 Binney J., Tremaine S., 2008, “Galactic Dynamics”, Princeton University Press, Princeton (BT08)
 Bond N.A., et al., 2009, arXiv 0909.0013
 Carlberg R.G., Sellwood J.A., 1985, ApJ, 292, 79
 Dale D.A., Giovanelli R., Haynes M.P., Campusano L.E., Hardy E., 1999, AJ, 118 1489
 Dehnen W., 1999, AJ, 118, 1201
 Dehnen W., Binney J., 1998, MNRAS, 298, 387
 Edvardsson B., Andersen J., Gustafsson B., Lambert DL., Nissen P.E., Tomkin J., 1993, A&A, 275 101
 Epchtein N., Simon G., Borsenberger J., de Batz B., Tanguy F., Begon S., Texier P., Derriere S., and the DENIS Consortium, 2005, “DENIS Catalogue third data release” <http://cdsweb.u-strasbg.fr/denis.html>
 Flynn C., Holmberg J., Portinari L., Fuchs B., Jahreiss H., 2006, MNRAS, 372, 1149
 Fuchs B. et al., 2009, AJ, 137, 4149 (14 authors)
 Fuhrmann K., 1998, A&A, 338, 161
 Gillessen S., Eisenhauer F., Trippe S., Alexander T., Genzel R., Martins F., Ott T., 2009, ApJ, 692, 1075
 Gilli G., Israelian G., Ecuivillon A., Santos N.C., Mayor M., 2006, A&A, 449, 723
 Gilmore G., Reid N., 1983, MNRAS, 202, 1025
 Gilmore G., Wyse R.F.G., Kuijken K., 1989, AnnRAA, 27, 555
 Holmberg J., Flynn C., 2000, MNRAS, 313, 209
 Holmberg J., Nordström B., Andersen J., 2007, A&A 475, 519
 Ivezić Z., et al., 2008, ApJ, 684, 287
 Juric M. et al., 2008, ApJ, 673, 864
 Kuijken K, Gilmore G., 1989, MNRAS, 239, 605
 Kuijken K, Gilmore G., 1991, ApJ, 367, L9
 Malhotra S., 1995, ApJ, 448, 138
 McMillan P.J., Binney J., 2009, MNRAS, submitted arXiv0907.4685
 Nordström B., Mayor M., Andersen J., Holmberg J., Pont F., Jørgensen B.R., Olsen E.H., Udry S., Mowlavi N., 2004, A&A, 418, 989
 Olling R.P., Dehnen W., 2003, ApJ, 599,275
 Perryman M.A.C., 1997, “The Hipparcos and Tycho Catalogues”, (Noordwijk: ESA Publications)
 Reddy B.E., Lambert D.L., Allende Prieto C., 2006, MNRAS, 367, 1329
 Reid M.J., Brunthaler A., 2004, ApJ, 616, 872
 Reid M.J., et al. (14 authors), 2009, ApJ, 700, 137
 Robin, A.C., Reylé, C., Derrière, S. & Picaud, S., 2003, A&A, 409, 523
 Schönrich R., Binney J., 2009, MNRAS, in press
 Shu F.H., 1969, ApJ, 158, 505
 Skrutskie M.F., et al., 2006, AJ, 131, 1163
 Spitzer L., 1942, ApJ, 95, 329
 Spitzer L., Schwarzschild M., 1953, ApJ, 118, 106
 Steinmetz et al., 2006, AJ, 132, 1645
 van der Kruit P.C., Searle L., 1982, A&A, 110, 61
 van Leeuwen F., 2007, *Hipparcos, the New Reduction of the Raw Data*, Springer Dordrecht
 Venn K.A., Irwin M., Shetrone M.D., Tout C.A., Hill V., Tolstoy E., 2004, AJ, 128, 1177
 Yanny B., et al., 2009a, AJ, 137, 4377
 Yanny B., et al., 2009b, arXiv:0902.1781
 Zacharias N., Urban S.E., Zacharias M.I., Wycoff G.L., Hall D.M., Monet D.G., Rafferty T.J., 2004, AJ, 127, 3043